Solution structure of the Ras-binding domain of RGL

Takanori Kigawa[a], Makoto Endo[a,b], Yutaka Ito[c], Mikako Shirouzu[a], Akira Kikuchi[d], Shigeyuki Yokoyama[a,b,*]

[a] *Cellular Signaling Laboratory, The Institute of Physical and Chemical Research (RIKEN), 2-1 Hirosawa, Wako, Saitama 351-0198, Japan*
[b] *Department of Biophysics and Biochemistry, Graduate School of Science, The University of Tokyo, 7-3-1 Hongo, Bunkyo-ku, Tokyo 113-0033, Japan*
[c] *Laboratory of Cellular and Molecular Biology, The Institute of Physical and Chemical Research (RIKEN), 2-1 Hirosawa, Wako, Saitama 351-0198, Japan*
[d] *Department of Biochemistry, Hiroshima University School of Medicine, 1-2-3 Kasumi, Minami-ku, Hiroshima, Hiroshima 734-8551, Japan*

Received 27 October 1998; received in revised form 26 November 1998

Abstract The RGL protein, a homolog of the Ral GDP dissociation stimulator (RalGDS), has been identified as a downstream effector of Ras. In the present study, the solution structure of the Ras-binding domain of RGL (RGL-RBD) was determined by NMR spectroscopy. The overall fold of RGL-RBD consists of a five-stranded β-sheet and two α-helices, which is the same topology as that of RalGDS-RBD. The backbone chemical shift perturbation of RGL-RBD upon interaction with the GTP analog-bound Ras was also examined. The solution structure of RGL-RBD, especially around some of the Ras-interacting residues, is appreciably different from that of RalGDS-RBD.

Key words: RGL; Ras-binding domain; GDP dissociation stimulator; Nuclear magnetic resonance; Solution structure; Signal transduction

1. Introduction

The Ras protein is a small GTP-binding protein that regulates cellular events such as proliferation and terminal differentiation [1]. In the GTP-bound state, Ras interacts with its downstream targets, which communicate with their partners located further downstream in the signaling pathways. The Raf kinase is one of these downstream targets of Ras [2–7], and the structure of the Ras-binding domain (RBD) has been determined [8,9]. Another group of Ras targets includes the GDP dissociation stimulators (GDS) for Ral, such as RalGDS [10] and RGL [11], and constitutes a large family [12]. Although there is no apparent sequence homology between Raf-RBD and RalGDS-RBD, they bind to the same region (the effector region) of Ras [10]. The structures of RalGDS-RBD have been determined [13,14], and it has been demonstrated that the overall fold of the RalGDS-RBD is similar to that of Raf-RBD. Thus, the RalGDS-RBD structure is classified within the ubiquitin superfold family [15], which also includes the Raf-RBD structure [8]. The largest structural differences between the Ras-free forms of Raf-RBD and RalGDS-RBD were found in the loop regions, the β1/β2 loop, the α1/β3 loop, and the α2/β5 loop [13,14].

The structures of the complex of Raf-RBD with a Ras homolog (the wild type and the E30D/K31E mutant of Rap1A) in the GMPPNP (an unhydrolyzable GTP analog)-bound form [9,16] and the complex of RalGDS-RBD with the GMPPNP-bound Ras (the E31K mutant) have been reported [17]. At the secondary structure level, the intermolecular interaction in the Raf-RBD•Rap1A(E30D/K31E)•GMPPNP complex is similar to that in the RalGDS-RBD•Ras(E31K)•GMPPNP complex; the β-sheets of the two interacting molecules form one continuous, extended β-sheet. In addition, the overall structures of Ras in the two RBD complexes are similar to each other and to that of the free Ras•GMPPNP [18]. However, there are significant differences between the two complexes at the tertiary structural level: (i) the relative orientation of RBD with respect to Ras/Rap1A is different, (ii) the electrostatic charge distribution at the interfaces is different, and (iii) the specific side-chain interactions are also different. These characteristics account for the different Ras/Rap1A-binding properties of Raf-RBD and RalGDS-RBD. For example, within Raf-RBD•Rap1A(E30D/K31E)•GMPPNP complex, Glu-31 of Rap1A(E30D/K31E) interacts with Arg-84 of Raf-RBD, located at the center of the α2 helix, while in the RalGDS-RBD•Ras(E31K)•GMPPNP complex, Lys-31 of Ras(E31K) interacts with Asp-815, Asn-818, and Asp-820 of RalGDS-RBD, located at the C-terminal end of the α2 helix and the α2/β3 loop. Consistently, Raf and Ral GDS have different affinities for Ras and Rap1A; the affinity of Raf-RBD for Ras is higher than that for Rap1A, whereas the affinity of RalGDS-RBD for Rap1A is higher than that for Ras [16,19].

RGL was initially identified as a target protein of Ras [11], and was found to interact with Ras in its C-terminal segment (residues 632–734; RGL-RBD) [20]. The residues of RalGDS-RBD that were found to interact with Ras [17] are not completely conserved in RGL-RBD, although the two RBDs have rather high overall sequence homology. In the present study, we determined the solution structure of RGL-RBD and identified its Ras-interacting residues by assigning the backbone signals in the complex with Ras.

2. Materials and methods

2.1. Sample preparation

The mouse RGL-RBD (residues 632–734) was expressed as a glutathione *S*-transferase (GST) fusion protein [20]. The unlabeled protein was obtained by culture of *Escherichia coli* BL21 cells in M9 minimal medium supplemented with $MgSO_4$ (3 mM), $CaCl_2$ (150 μM), trace element solution [$ZnSO_4$ (4 μM), $MnSO_4$ (1 μM), H_3BO_3 (4.7 μM), $CuSO_4$ (0.7 μM), $CaCl_2$ (2.5 μM), and $FeCl_3$ (1.8 μM)] [21], and ampicillin (0.05 mg/ml). The uniformly ^{15}N- or $^{13}C/^{15}N$-labeled proteins were produced in a similar manner, except for the use of $^{15}NH_4Cl$ (1 g/l, Isotec) as the sole nitrogen source and/or [$^{13}C_6$]D-glucose (2 g/l, Isotec) as the sole carbon source. To prepare the

*Corresponding author. Fax: (81) (48) 462 4675.
E-mail: yokoyama@y-sun.biochem.s.u-tokyo.ac.jp

Abbreviations: DTT, dithiothreitol; GDS, GDP dissociation stimulator; GMPPNP, guanosine 5′-*O*-(β,γ-imidotriphosphate); GST, glutathione *S*-transferase; RBD, Ras-binding domain

PII: S0014-5793(98)01596-8

~50% randomly deuterated and uniformly $^{13}C/^{15}N$-labeled protein, the cell was adapted to growth in $^{2}H_2O$ as reported previously [22] and was grown in a similar manner, except that M9 medium (60% $^{2}H_2O$/40% $^{1}H_2O$) was used instead. Harvested cells were suspended in 50 mM Tris-HCl buffer (pH 7.5) containing 5 mM dithiothreitol (DTT) and 2% Triton X-100, and were disrupted by sonication. After centrifugation, the supernatant was loaded onto a glutathione-Sepharose 4B column (Pharmacia Biotech) equilibrated with 50 mM Tris-HCl buffer (pH 7.5) containing 5 mM DTT. The bound GST•RGL-RBD fusion protein was eluted with 50 mM Tris-HCl buffer (pH 8.0) containing 10 mM glutathione, and then was dialyzed against Tris-HCl buffer (pH 8.0). The fusion protein was cleaved with thrombin (Sigma) for 5 h at 25°C, and then was applied to a DEAE Sephacel column (Pharmacia Biotech) equilibrated with 50 mM Tris-HCl buffer (pH 7.5) containing 2 mM DTT and 1 mM PMSF. The RGL-RBD was eluted with an NaCl gradient (0–350 mM). The purified RGL-RBD was verified by SDS-PAGE, mass spectrometry, and N-terminal sequencing.

For the RGL-RBD•Ras complex, we used truncated forms of the wild type and the mutant (D30E/E31K) of the human Ha-Ras protein consisting of residues 1–171. The purification of the Ras samples was achieved as described previously [23–25]. A GTP analog, guanosine 5′-*O*-(β,γ-imidotriphosphate) (GMPPNP), which is much more slowly hydrolyzed than GTP in the complex with Ras, was used in order to maintain the active GTP-bound form during the NMR measurements. Exchange of the Ras-bound guanine nucleotide was performed as described previously [26].

The buffer for the RGL-RBD solution (1.5 mM) was finally exchanged for 90% $^{1}H_2O$/10% $^{2}H_2O$ NMR buffer containing 50 mM Tris-HCl (pH 7.5), 5 mM DTT, and 200 mM NaCl, using a Centricon-3 concentrator (Amicon). The titration experiment was performed using ^{15}N-labeled RGL-RBD and unlabeled Ras (wild type)•GMPPNP or Ras(D30E/E31K)•GMPPNP (RGL-RBD: Ras molar ratios of 1:0.5, 1:1, 1:1.5, and 1:2) in 90% $^{1}H_2O$/10% $^{2}H_2O$ NMR buffer containing 50 mM Tris-HCl (pH 7.5), 5 mM DTT, 10 mM $MgCl_2$, and 200 mM NaCl. As the sample for the RGL-RBD•Ras complex analysis, 1.0 mM of the ~50% $^{2}H/^{13}C/^{15}N$ RGL-RBD was used to lengthen the transverse relaxation times of the ^{1}HN and ^{13}C nuclei and to increase the sensitivity in the triple resonance experiments [27,28]. This sample was mixed with the Ras(D30E/E31K)•GMPPNP at a 1:2 molar ratio in 90% $^{1}H_2O$/10% $^{2}H_2O$ NMR buffer containing 50 mM Tris-HCl (pH 7.5), 5 mM DTT, 10 mM $MgCl_2$, and 200 mM NaCl.

2.2. NMR spectroscopy and structure determination

All NMR experiments were performed at 25°C on a Bruker AMX600 or DMX500 spectrometer equipped with a pulsed field gradient unit. All of the experiments detecting amide proton signals used the water flip-back pulses [29], because the samples were under neutral pH conditions. This allowed us to identify the slowly exchanging amide protons from the nuclear Overhauser effects (NOEs) between the amide protons and waters. The indirect dimensions of the 3D spectra were processed with a two-dimensional maximum entropy algorithm [30] using Azara software (Wayne Boucher, unpublished). The spectra were analyzed with the FELIX software (MSI) in combination with in-house macro programs (T. Terada, unpublished). The backbone ^{1}H, ^{13}C, and ^{15}N resonances of the free form of RGL-RBD were assigned using the uniformly $^{13}C/^{15}N$-labeled sample from a series of 3D experiments (HNCA [31], HN(CO)CA [32], HNCACB [33], and 3D CBCA(CO)NH [34]). The side chain resonance assignments, including the stereospecific assignments and 23 χ^1 angle restraints of the β-methylene groups and the valine methyl groups, were obtained from the 3D ^{15}N-edited TOCSY (mixing time of 45 ms) [35], HNHB [36], and HCCH-TOCSY (mixing time of 16 ms) [37] spectra. A total of 1253 distance restraints, obtained from the ^{15}N-edited NOESY (mixing time of 120 ms) [35] and ^{13}C-edited NOESY (mixing time of 120 ms) [38] spectra, were given upper bounds of 2.8, 3.4, 4.6, and 5.8 Å (2.9, 3.6, 4.6, and 5.8 Å for NOEs involving NH protons) based on the NOE intensities. The 42 hydrogen bond restraints within the secondary structure elements, obtained from an analysis of the slowly exchanging amide protons, and 31 ϕ angle restraints obtained from the chemical shift index analysis [39], were also employed. The structure calculations were carried out using the simulated annealing protocol [40] with X-PLOR 3.1 [41] on Indigo^2 or O2 workstations (Silicon Graphics). The backbone ^{1}H, ^{13}C, and ^{15}N resonances of the RGL-RBD complexed with Ras(D30E/E31K)•GMPPNP were assigned from deuterium-decoupled 3D experiments (HNCA [42] and HN(CO)CA [43]) using the ~50% $^{2}H/^{13}C/^{15}N$-labeled RGL-RBD. Structure figures were generated using the programs Molscript [44] and MOLMOL [45].

3. Results and discussion

3.1. Structure determination

The RGL-RBD sample at a high concentration (>1.0 mM) is not stable under conditions below pH 6.5 or 150 mM NaCl, in our experience. Therefore, all of the NMR experiments were performed under neutral pH (pH 7.5) and relatively high ionic strength conditions (200 mM NaCl). Sequence-specific assignments of the ^{1}HN, ^{15}N, $^{13}C\alpha$, $^{1}H\alpha$, $^{13}C\beta$, and $^{1}H\beta$ resonances of the non-proline residues were obtained, except for Ser-632, Ser-635, Asn-643, Asn-659, and Asn-660. No backbone resonances of these residues were observed in any experiment used in this study to detect amide proton signals (see Section 2). These residues are located in the N-terminal region or the β1/β2 loop. The lack of signals from these residues was due to exchange broadening under neutral pH conditions.

As the first step of the structure determination, the secondary structure of RGL-RBD was determined on the basis of the NOE data involving the backbone protons and the slow exchange properties of the hydrogen-bonded amide protons identified from the NOE data to/from water (Fig. 1). This was further confirmed by the chemical shift index analysis [39]. The N-terminal region (residues 632–646) appears to be highly flexible, as only a small number of inter-residue NOEs could be detected. Then, the structure calculations were performed for residues 647–734. The structure of RGL-RBD was

Table 1
Structural statistics

	Selected structures[a]	Minimized averaged structure[b]
X-PLOR energies (kcal/mol)		
*E*total	194 ± 2	193
*E*bond	7.79 ± 0.40	8.20
*E*angle	120 ± 2	121
*E*improper	17.3 ± 0.6	18.1
*E*vdw	25.4 ± 1.0	22.2
*E*noe	24.2 ± 1.7	24.3
*E*cdih	0.14 ± 0.13	0.01
*E*l-j	−102 ± 33	−61
Rms deviations from idealized geometry		
bonds (Å)	0.002 ± 0.000	0.002
angles (°)	0.56 ± 0.005	0.56
impropers (°)	0.40 ± 0.007	0.41
Rms deviations from experimental restraints		
distance (Å)	0.019 ± 0.001	0.019
dihedral (°)	0.18 ± 0.09	0.06
Rms deviations from the mean structure		
	backbone	all heavy
All residues	1.06 ± 0.13	1.59 ± 0.15
Secondary structure elements except for the α2	0.60 ± 0.17	1.18 ± 0.20

[a]Final 20 simulated annealing structures.
[b]The structure obtained by restrained regularization of the mean structure calculated by averaging the coordinates of the 20 individual SA structures.

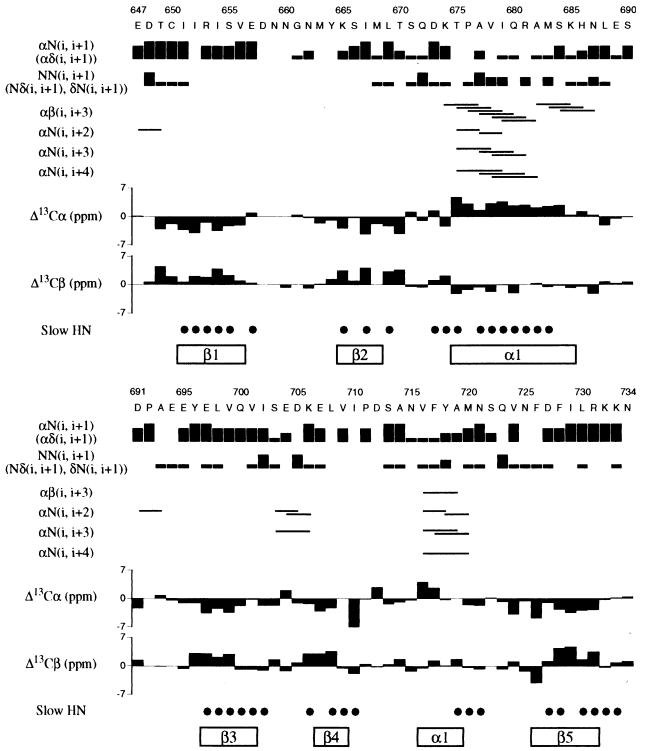

Fig. 1. Summary of the short- and medium-range NOEs, slow exchange amide protons, and $^{13}C_\alpha$ and $^{13}C_\beta$ secondary shifts ($\Delta 13C_\alpha$ and $\Delta 13C_\beta$) for residues 647–734. NOE connectivities are marked by closed bars and solid lines. Filled circles indicate residues with slowly exchanging amide protons. Secondary structure elements are also shown.

determined from a total of 1349 experimental restraints (see Section 2). The structural statistics for the final simulated annealing structures are summarized in Table 1. Fig. 2a shows 20 backbone structures, which were aligned by superimposing the backbone atoms (N, Cα, and C′) of the secondary structure elements. A ribbon representation of the tertiary structure of RGL-RBD is shown in Fig. 2b. The structure of RGL-RBD consists of five β-strands, one long α-helix, and an additional one-turn helix, arranged as β-β-α-β-β-α-β. The β1/β2 loop and the region around the α2 helix are not well defined as compared with the other regions of the molecule, because only a few long-range NOEs were observed for these regions. The ensemble of structures will be deposited in the Brookhaven Protein Data Bank. The average rms deviation for the backbone atoms was 1.06 ± 0.13 Å for all regions, and 0.60 ± 0.17 Å for the secondary structure elements, except for the α2 helix. The hydrophobic core is formed by residues Ile-652, Ile-654, Val-656, Ile-667, Pro-676, Val-678, Ile-679, Ala-682, Met-683, Leu-688, Pro-692, Leu-698, Ile-702, Leu-708, Pro-711, Phe-717, Phe-726, Phe-728, and Leu-730. Many of these residues, which exist either on the β-strands (β1–β5) or on/around the α1 helix, anchor the α1 helix onto the β-sheet. In addition, many of these hydrophobic residues are well conserved among the RBDs of the RalGDS family [12], indicating that the hydrophobic interactions between these residues are important for the proper folding of these domains.

3.2. Comparison with other RBDs

As expected from the high sequence similarity, the overall fold of RGL-RBD is similar to that of RalGDS-RBD [13,14] (Fig. 2), except for the short 3_{10} helix identified by the X-ray crystallography study [14], being classified in the ubiquitin superfold family [15]. When compared in detail with the free-form RalGDS-RBD structure, large differences are found for residues 667–674 and 702–725, resulting in a weaker twist of the β-sheet of RGL-RBD than that of RalGDS-RBD (Fig. 2b,c). There are also large differences in the connecting loop structures involving residues 657–664 and 686–696. These differences are because the amino acid sequences in these regions are less homologous between RGL-RBD and RalGDS-RBD than in the other regions (Fig. 2d).

In the RalGDS-RBD structure determined by X-ray crystallography [14], RBD forms a homodimer by an intermolecular disulfide bond and the intermolecular anti-parallel β-sheet. As a result, the β1 and β2 strands are more extended than those in the RGL-RBD structure determined in this study and the RalGDS-RBD structure determined by NMR spectroscopy [13] (Fig. 2d). RGL-RBD is not stable in a low ionic strength solution, as noted above, and removal of the N-terminal unstructured part of the RalGDS-RBD protein improved the stability [13]. These findings suggest that RGL-RBD and RalGDS-RBD interact with each other, probably electrostatically, through the N-terminal unstructured part and form a homodimer.

3.3. Interaction of RGL-RBD with Ras•GMPPNP

First, we monitored the chemical shift change and the line broadening of the ^1H-^{15}N HSQC cross peaks of the ^{15}N-labeled RGL RBD during the titration with unlabeled Ras(wt)•GMPPNP. At the 0.5:1 molar ratio, a set of broader cross peaks appeared in addition to the sharper cross peaks due to the free form of RGL-RBD. At the 2:1 molar ratio, some of the cross peaks of the free form became weak, although none disappeared. This result indicates that the interaction between RGL-RBD and Ras•GMPPNP occurs by slow exchange on the NMR time scale, as shown in the case of the Raf-RBD and Ras interaction (T. Terada, unpublished). The titration experiment with the Rap1A-type mutant Ras(D30E/E31K)•GMPPNP was also examined, because RGL-RBD, as well as RalGDS-RBD [16,46,47], binds more tightly with Ras(E31K)•GMPPNP or Ras(D30E/E31K)•GMPPNP than with Ras(wt)•GMPPNP (M. Shirouzu, unpublished). In this case, a set of broader cross peaks also appeared at the 0.5:1 molar ratio. At the 2:1 molar ratio, some of the cross peaks of the free form disappeared. The broader cross peaks that appeared in the titration with Ras(D30E/E31K)•GMPPNP coincide with those of the Ras(wt)•GMPPNP complex. Thus, Ras(D30E/E31K)•GMPPNP was used for further analysis of the complexed state of RGL-RBD.

For the backbone resonance assignment of the complexed state of RGL RBD, randomly fractional deuterated (~50%) RGL-RBD was mixed with unlabeled Ras(D30E/E31K)•GMPPNP at a 1:2 molar ratio. The ^1HN, ^{15}N, and $^{13}C_\alpha$ resonances of RGL-RBD were sequence-specifically assigned for the non-Pro residues, except for residues 658–660, and 730. The chemical shift change Δ for each residue was calculated as the average of the chemical shift changes in Hz units observed at 14.1 T (the ^1H frequency is 600 MHz) of ^1HN and ^{15}N: $[(1/2)\{\delta(^1HN)^2+\delta(^{15}N)^2\}^{1/2}]$, where $\delta(x)$ is the chemical shift difference in Hz for resonance nucleus x be-

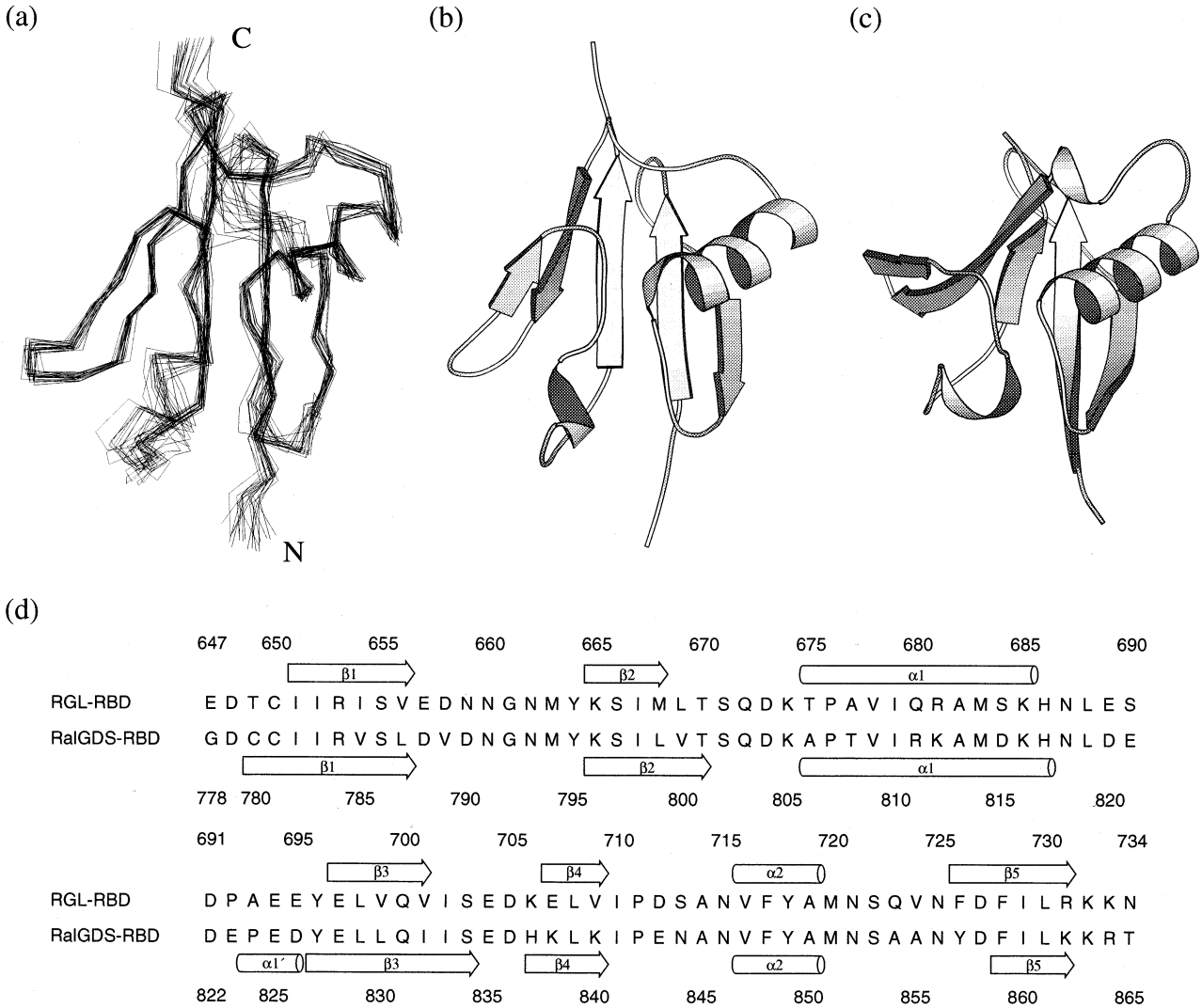

Fig. 2. a: Superposition of the ensemble of the final 20 simulated annealing structures of RGL-RBD. b: Ribbon representation of the minimized averaged structure of RGL-RBD. c: Ribbon representation of RalGDS-RBD (PDB accession code; 1LXD). d: Sequence alignment of RGL-RBD (mouse) and RalGDS-RBD (rat). Secondary structure elements for RGL-RBD and RalGDS-RBD [14] are shown above and below the sequences, respectively.

tween the free and the complexed states. On average, the chemical shift changes were relatively larger than in the case of Raf-RBD binding with Ras (T. Terada, unpublished). Large changes ($\Delta \geq 120$ Hz) were observed for residues Arg-653, Ile-654, Tyr-664, Lys-665, Ile-667, Met-668, Ile-679, and His-686, and relatively large changes (40 Hz $\leq \Delta < 120$ Hz) occurred for a broad range of residues (Fig. 3a,b).

As reported for the RalGDS-RBD•Ras complex structure [17], RalGDS-RBD interacts with Ras mainly by forming an intermolecular β-sheet through its β2 with the β2 of Ras, which includes the effector (switch I) region (residues 32–40). There are also electrostatic interactions with the effector region of Ras, indicating that the interaction interface of RalGDS-RBD for Ras is formed by β1, β2, the C-terminal part of α1, and the N-terminal part of the α1/β3 loop. In this study, chemical shift changes upon binding with Ras were found in the corresponding region of RGL-RBD, as noted above. Thus, the Ras-binding interface of RGL-RBD is formed by the same region as that of RalGDS-RBD. In addition to the residues on this interaction interface, changes were also observed for the hydrophobic core-forming residues and its neighbors of RGL-RBD, indicating that conformational changes occur not only on the interaction interface but also on the hydrophobic core of the molecule. This phenomenon was also found in the case of complex formation of Ras with Raf-RBD (T. Terada, unpublished) and RasGDS-RBD [13].

A hydrogen bond between the side chain guanido group of Arg-811 and the main chain carbonyl group of Asp-822 is found on RalGDS-RBD in the complex form, but not in the free form (Fig. 4b,c). By this hydrogen bond formation, Asn-818 and Asp-820 on the α1/β3 loop are pulled near Asp-815 on the α1 helix, and then, the binding site for residue 31 of Ras is formed. In the RGL-RBD case, Glu-689 (the counterpart of Asp-820 of RalGDS-RBD) is much farther away from Gln-680 (the counterpart of Arg-811 of RalGDS-RBD) (Fig. 4a). Thus, the binding site for residue 31 of Ras may be formed by Ser-684 and Asn-687, resulting in a weaker inter-

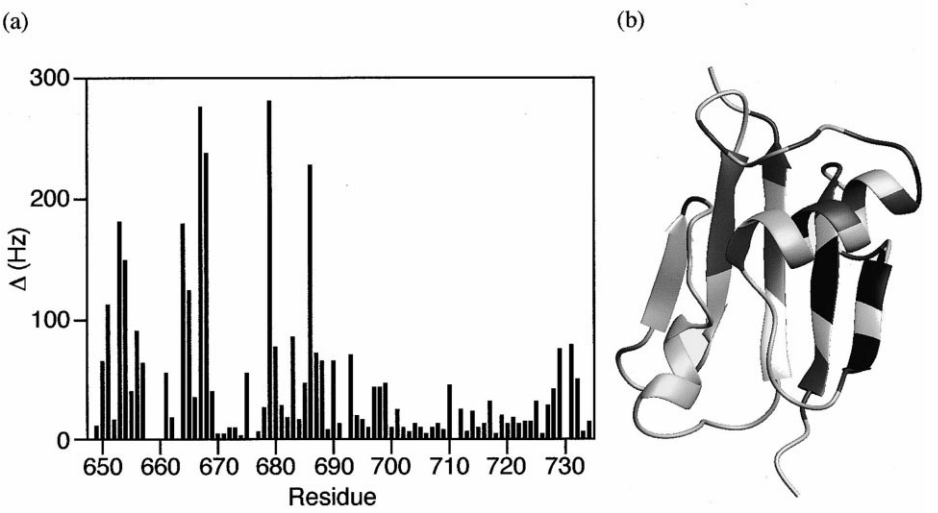

Fig. 3. Chemical shift perturbation of backbone ^{1}HN and ^{15}N nuclei of RGL-RBD upon binding with Ras(D30E/E31K)•GMPPNP. a: Plots of the mean shift difference Δ (Hz) for each amino acid residue calculated as described in the text. b: Mapping Δ on the ribbon representation of RGL-RBD. Light gray (Δ < 40, proline, and residues with unassigned backbone chemical shifts); medium gray (40 ≤ Δ < 120); black (Δ ≥ 120).

action between residue 31 of Ras and RGL. This accounts for the result that the E31K mutation of Ras increases the affinity more for RalGDS-RBD than for RGL-RBD (M. Shirouzu, unpublished).

In conclusion, the present study has revealed an appreciable difference in the functional structures for the Ras/Rap1A interaction, between the homologous pair of RalGDS-RBD and RGL-RBD. In other words, although the folds of both RalGDS-RBD and RGL-RBD belong to the same ubiquitin superfold family, their Ras/Rap1A interaction interfaces are differentially fine-tuned at the tertiary structure level. This is certainly due to the small number of amino acid replacements in the highly homologous sequences. On the basis of the flexibility and tunability of the ubiquitin-like fold, we propose that many homologs belonging to this superfold family [12] are likely to have differentiated in similar sophisticated manners at the tertiary structure level, for their distinct and specific roles in cells.

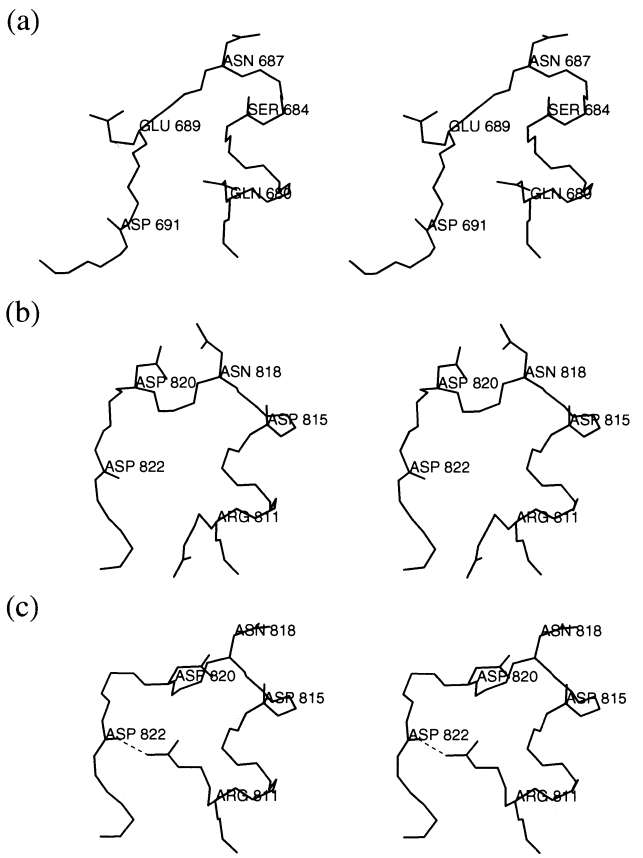

Fig. 4. The binding site for residue 31 of Ras. a: The free-form RGL-RBD determined in this study. b: The free-form RalGDS-RBD (PDB code; 1LXD). c: The RalGDS-RBD complexed with Ras(E31K)•GMPPNP (the coordinates were kindly provided by Prof. S.-H. Kim).

Acknowledgements: We thank K. Iwahori, T. Morita, and M. Ikuta (University of Tokyo/RIKEN) for preparation of protein samples, Drs. K. Takio and N. Dohmae (RIKEN) for performing mass spectrometry and N-terminal amino acid analyses, T. Terada (University of Tokyo/RIKEN) for providing macros of the FELIX package, and Prof. S.-H. Kim (University of California) for providing the coordinates of the RalGDS-RBD•Ras(E31K)•GMPPNP complex. This work was supported in part by research grants from RIKEN.

References

[1] Barbacid, M. (1987) Annu. Rev. Biochem. 56, 779–827.
[2] Moodie, S.A., Willumsen, B.M., Weber, M.J. and Wolfman, A. (1993) Science 260, 1658–1661.
[3] Zhang, X.-F. et al. (1993) Nature 364, 308–313.
[4] Warne, P.H., Viciana, P.R. and Downward, J. (1993) Nature 364, 352–355.
[5] Van Aelst, L., Barr, M., Marcus, S., Polverio, A. and Wigler, M. (1993) Proc. Natl. Acad. Sci. USA 90, 6213–6217.
[6] Vojtek, A.B., Hollenberg, S.M. and Cooper, J.A. (1993) Cell 74, 205–214.
[7] Koide, H., Satoh, T., Nakafuku, M. and Kaziro, M. (1993) Proc. Natl. Acad. Sci. USA 90, 8683–8686.
[8] Emerson, S.D. et al. (1995) Biochemistry 34, 6911–6918.
[9] Nassar, N., Horn, G., Herrmann, C., Scherer, A., McCormick, F. and Wittinghofer, A. (1995) Nature 375, 554–560.
[10] Hofer, F., Fields, S., Schneider, C. and Martin, G.S. (1994) Proc. Natl. Acad. Sci. USA 91, 11089–11093.
[11] Kikuchi, A., Demo, S.D., Ye, Z.H., Chen, Y.W. and Williams, L.T. (1994) Mol. Cell. Biol. 14, 7483–7491.

[12] Ponting, C.P. and Benjamin, D.R. (1996) Trends Biochem. Sci. 21, 422–425.
[13] Geyer, M., Herrmann, C., Wohlgemuth, S.B., Wittinghofer, A. and Kalbitzer, H.R. (1997) Nature Struct. Biol. 4, 694–699.
[14] Huang, L., Weng, X., Hofer, F., Martin, G.S. and Kim, S.-H. (1997) Nature Struct. Biol. 4, 609–615.
[15] Orengo, C.A., Jones, D.T. and Thornton, J.M. (1994) Nature 372, 631–634.
[16] Nassar, N., Horn, G., Herrmann, C., Block, C., Janknecht, R. and Wittinghofer, A. (1996) Nature Struct. Biol. 3, 723–729.
[17] Huang, L., Hofer, F., Martin, G.S. and Kim, S.H. (1998) Nature Struct. Biol. 5, 422–426.
[18] Milburn, M.V., Tong, L., deVos, A.M., Brunger, A., Yamaizumi, Z., Nishimura, S. and Kim, S.H. (1990) Science 247, 939–945.
[19] Block, C., Janknecht, R., Herrmann, C., Nassar, N. and Wittinghofer, A. (1996) Nature Struct. Biol. 3, 244–251.
[20] Koyama, S., Chen, Y.W., Ikeda, M., Muslin, A.J., Williams, L.T. and Kikuchi, A. (1996) FEBS Lett. 380, 113–117.
[21] Kim, H.W., Perez, J.A., Ferguson, S.J. and Campbell, I.D. (1990) FEBS Lett. 272, 34–36.
[22] Yamazaki, T., Lee, W., Revington, M., Mattiello, D.L., Dahlquist, F.W., Arrowsmith, C.H. and Kay, L.E. (1994) J. Am. Chem. Soc. 116, 6464–6465.
[23] Yamasaki, K., Muto, Y., Ito, Y., Wälchli, M., Miyazawa, T., Nishimura, S. and Yokoyama, S. (1992) J. Biomol. NMR 2, 71–82.
[24] Muto, Y. et al. (1993) J. Biomol. NMR 3, 165–184.
[25] Ito, Y. et al. (1997) Biochemistry 36, 9109–9119.
[26] Yamasaki, K., Kawai, G., Ito, Y., Muto, Y., Fujita, J., Miyazawa, T., Nishimura, S. and Yokoyama, S. (1989) Biochem. Biophys. Res. Commun. 162, 1054–1062.
[27] Yamazaki, T., Lee, W., Arrowsmith, C.H., Muhandiram, D.R. and Kay, L.E. (1994) J. Am. Chem. Soc. 116, 11655–11666.
[28] Grzesiek, S., Anglister, J., Ren, H. and Bax, A. (1993) J. Am. Chem. Soc. 115, 4369–4370.
[29] Grzesiek, S. and Bax, A. (1993) J. Am. Chem. Soc. 115, 12593–12594.
[30] Laue, E.D., Mayger, M.R., Skilling, J. and Staunton, J. (1986) J. Magn. Reson. 68, 14–29.
[31] Kay, L.E., Ikura, M., Tschudin, R. and Bax, A. (1990) J. Magn. Reson. 89, 496–514.
[32] Bax, A. and Ikura, M. (1991) J. Biomol. NMR 1, 99–104.
[33] Wittekind, M. and Mueller, L. (1993) J. Magn. Reson. Ser. B 101, 201–205.
[34] Grzesiek, S. and Bax, A. (1992) J. Am. Chem. Soc. 114, 6291–6293.
[35] Marion, D., Driscoll, P.C., Kay, L.E., Wingfield, P.T., Bax, A., Gronenborn, A.M. and Clore, G.M. (1989) Biochemistry 28, 6150–6156.
[36] Archer, S.J., Ikura, M., Torchia, D.A. and Bax, A. (1991) J. Magn. Reson. 95, 636–641.
[37] Bax, A., Clore, G.M. and Gronenborn, A.M. (1990) J. Magn. Reson. 88, 425–431.
[38] Muhandiram, D.R., Farrow, N.A., Xu, G.-Y., Smallcombe, S.H. and Kay, L.E. (1993) J. Magn. Reson. Ser. B 102, 317–321.
[39] Wishart, D.S. and Sykes, B.D. (1994) J. Biomol. NMR 4, 171–180.
[40] Nilges, M., Clore, M. and Gronenborn, A.M. (1991) FEBS Lett. 239, 129–136.
[41] Brünger, A.T. (1993) XPLOR Version 3.1: A System for X-ray Crystallography and NMR, Yale University Press, New Haven, CT.
[42] Yamazaki, T., Lee, W., Revington, M., Mattiello, D.L., Dahlquist, F.W., Arrowsmith, C.H. and Kay, L.E. (1994) J. Am. Chem. Soc. 116, 6464–6465.
[43] Yamazaki, T., Lee, W., Arrowsmith, C.H., Muhandiram, D.R. and Kay, L.E. (1994) J. Am. Chem. Soc. 116, 11655–11666.
[44] Kraulis, P.J. (1991) J. Appl. Crystallogr. 24, 946–950.
[45] Koradi, R., Billeter, M. and Wüthrich, K. (1996) J. Mol. Graph. 14, 51–55.
[46] Herrmann, C., Horn, G., Spaargaren, M. and Wittinghofer, A. (1996) J. Biol. Chem. 271, 6794–6800.
[47] Shirouzu, M. et al. (1998) J. Biol. Chem. 273, 7737–7742.